# Performance of Sixth-order Finite Surface Method in Turbulent Flow Simulations

IOP Conf. Series: Materials Science and Engineering **501** (2019) 012044 doi:10.1088/1757-899X/501/1/012044

# Performance of Sixth-order Finite Surface Method in Turbulent Flow Simulations

**A Hokpunna**[1*]

[1*] Mechanical Engineering Department, Faculty of Engineering,
Chiang Mai University, 239 Huaykaew Rd., Chiang Mai, Thailand 50200

* Corresponding Author: E-mail arpiruk.hok@eng.cmu.ac.th

**Abstract:** This paper presents the finite-surface method for solving the Navier-Stokes equations (NSE). This method defines the velocities as a surface-averaged value on the surfaces of the pressure cells. Consequently, the mass conservation on the pressure cells becomes an exact equation. The only things left to approximate is the momentum equation and the pressure at the new time step. At certain conditions, the exact mass conservation enables the explicit n-th order accurate NSE solver to be used with the pressure treatment that is two or four order less accurate without losing the apparent convergence rate. This feature was not possible with finite volume of finite difference methods. The convergence rate for laminar flows are presented. In addition to these result which was already presented elsewhere, this work presents a resolution criteria needed to achieve a DNS-like solution. The turbulent channel flow with friction Reynolds number 590 is used in this study. Previously, it was found that a fourth-order scheme is effectively 10X faster than the second-order scheme, at the comparable accuracy. The newly developed sixth-order FSM is 4X faster than the fourth-order scheme and thus it is a very interesting numerical method for solving turbulent flow. This speedup is possible due to the reduction of the number of grid points.

## 1. Introduction

Finite Volume Method (FVM) and Finite Difference Method (FDM) have been important tools for turbulence research. In the past three decades, numerous higher-order methods have been developed. Despite having significant higher cost, they outperformed the low-order methods in both accuracy and performance in three-dimensional problems. The main reason is because higher-order methods require less number of grid points and this reduction is a quartic function (including time-step) while the cost function is a linear one. This advantage is well observed in convection and diffusion problems. Early applications of higher-order scheme to the incompressible Navier-Stokes equations (NSE) often improved the approximation of the convection and diffusion terms, but kept the approximation of pressure and the Poisson equation to second order. This was partly due to the pressure can be viewed as a Lagrange multiplier and thus it should not affect the accuracy of the momentum. Another reason is because higher-order treatment of the pressure is difficult. Later it was shown that the n-th order NSE solver must be used with the same order pressure [1,2]. This higher-order treatment of the pressure demands more computing power than the momentum equation. In fourth-order context, the Poisson's

stencil is 7-point wide in 1D and the 3D Laplacian matrix is 19-banded. Comparing to the stencils of the standard second-order scheme (7-band in 3D), while the matrix of the sixth-order momentum is only tridiagonal. Thus reducing the complexity of the Poisson equation is crucial to simulation performance.

This paper presents a newly developed method called Finite-Surface Method (FSM). It fills the gap between FDM, and the FVM in which they define the data as point and volumes, respectively. FSM treats surface-averaged values as the flow unknown. The Poisson equation generated by FSM is significantly smaller than both FDM and FVM. This can be mistaken as the scheme IV of Van Leer [19] in which he proposed to improve the accuracy by using the boundary values together with the cell-averaged as the flow variables. In the same spirit, Sun and Xiao developed the multi-moment method in [3]. Hybridizible discontinuous Galerkin method also defines boundary polynomials in addition to the cell polynomial and use them to solve the instabilities in diffusion problem. These methods then compute numerical fluxes from the polynomial defined by these different types of data. At best, the mass imbalance of the cell is only exact up to the polynomial being used. The FSM presented here deliver a literally exact mass imbalance because the field variables are defined as the surface-averaged at the cell-surface. Our FSM approach, defines the velocities on these control surfaces and keep the pressure defined on the original cells. It is clear that the sum of these velocity fluxes is the exact integral of the divergence on the pressure cell. This exact mass balance can be computed at the same cost as the traditional second-order scheme. Furthermore, the positioning, of the data is still the same as they were on the staggered grid and thus half-a-cell advantage of the staggered grid in calculating the pressure gradient is maintained. Ultimately, all the advantages of the staggered grid are kept without any need to actually define the staggered cells or co-volumes at all. This approach also delivers the most compact discrete Poisson operator L under the projection method which greatly simplifies the treatment of pressure using explicit scheme. Furthermore, the simplicity of the mass conservation equation allows compact treatments of the pressure at virtually the same cost as the explicit scheme. Therefore, the finite surface method is very attractive.

## 2. The Navier-Stokes equations

The integral form of the incompressible Navier-Stokes equations for incompressible Newtonian fluid can be written as

$$\oint \boldsymbol{u} \cdot \boldsymbol{n}\, dA = 0 \tag{1}$$

$$\frac{\partial}{\partial t}\int_{\Omega} \boldsymbol{u}\, d\Omega + \oint_A (\boldsymbol{u} \cdot \boldsymbol{n})\boldsymbol{u}\, dA = \nu \oint_A \boldsymbol{T}\, dA - \frac{1}{\varrho}\oint_A p\boldsymbol{I} \cdot \boldsymbol{n}\, dA \tag{2}$$

Here, the variables and notations are velocity vector:u, pressure:p, strain rate tensor:T, identity matrix:I, density: $\varrho$ and the kinematic viscosity: $\nu$. The unit vector ($\mathbf{n}$) of an infinitesimal area dA is pointing outwards of the volume $d\Omega$.

FSM discretizes the continuous domain to a discrete domain where the momentum variables are defined on the area normal to its direction while the pressure is defined as the averaged quantity over the cells. Such arrangement allows **an exact evaluation of mass imbalance over the pressure cell**. This exact imbalance can be calculated easily and efficiently. It only cost 5 floating point operations (FP) while the standard sixth-order approximation of the divergence costs 35 FP.

Such physical discretization requires a special integral form of equations (1) and (2) and the discrete form of the NSE under finite-surface method is displayed in figure 1. The square brackets represent the average and its superscript is the plane of averaging. Note that the indices *ijk* indicates the center of the pressure cells. The staggered indices e.g. *js* is the midpoint between the *j* and *j+1*. Please note that the position of *js* and *js+1/2* are the same.

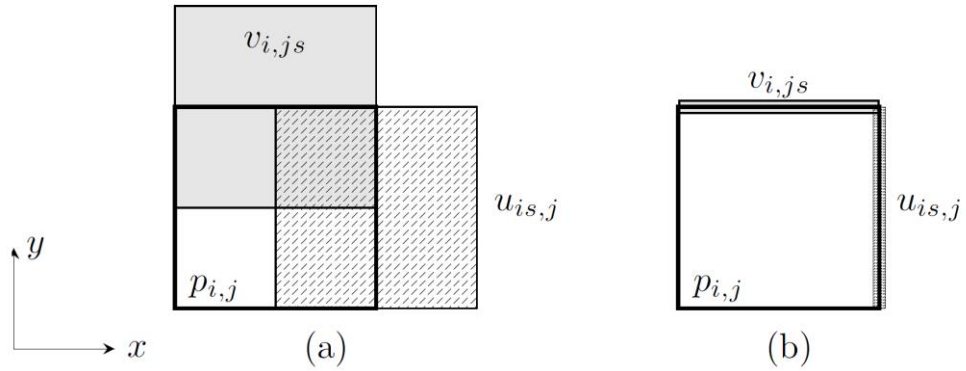


**Figure 1.** Spatial discretization of FSM. FSM shrinks the momentum control volume of standard FVM to the control surface of the pressure cell.

$$
\begin{aligned}
[div]^{xyz}_{i,j,k}\triangle x_i\triangle y_j\triangle z_k &= \left([u]^{yz}_{i+\frac{1}{2},j,k} - [u]^{yz}_{i-\frac{1}{2},j,k}\right)\triangle y_j\triangle z_k \\
&+ \left([v]^{xz}_{i,j+\frac{1}{2},k} - [v]^{xz}_{i,j-\frac{1}{2},k}\right)\triangle x_i\triangle z_k \\
&+ \left([w]^{xy}_{i,j,k+\frac{1}{2}} - [w]^{xy}_{i,j,k-\frac{1}{2}}\right)\triangle x_i\triangle y_j
\end{aligned}
$$

$$
A_{j,k}\frac{\partial[u]^{yz}_{is,j,k}}{\partial t} = -\mathcal{C}_{is,j,k} + \nu\mathcal{D}_{is,j,k} - \frac{1}{\rho}\mathcal{P}_{is,j,k}
$$

$$
\begin{aligned}
\mathcal{C}_{is,j,k} = \left[\frac{\partial uu}{\partial x}\right]^{yz}_{is,j,k}\triangle y_j\triangle z_k &+ \left([vu]^{z}_{is,j+\frac{1}{2},k} - [vu]^{z}_{is,j-\frac{1}{2},k}\right)\triangle z_k \\
&+ \left([wu]^{y}_{is,j,k+\frac{1}{2}} - [wu]^{y}_{is,j,k-\frac{1}{2}}\right)\triangle y_j,
\end{aligned}
$$

$$
\begin{aligned}
\mathcal{D}_{is,j,k} = \left[\frac{\partial^2 u}{\partial x^2}\right]^{yz}_{is,j,k}\triangle y_j\triangle z_k &+ \left(\left[\frac{\partial u}{\partial y}\right]^{z}_{is,j+\frac{1}{2},k} - \left[\frac{\partial u}{\partial y}\right]^{z}_{is,j-\frac{1}{2},k}\right)\triangle z_k \\
&+ \left(\left[\frac{\partial u}{\partial z}\right]^{y}_{is,j,k+\frac{1}{2}} - \left[\frac{\partial u}{\partial z}\right]^{y}_{is,j,k-\frac{1}{2}}\right)\triangle y_j,
\end{aligned}
$$

**Figure 2.** Discrete Navier-Stokes equation of FSM

## 3. Numerical Approximations

In this work we use compact sixth-order schemes from Lele [4] and Kobayashi [5] as well as a nonlinear correction concept from [1]. The numerical approximations are presented here only for *u*. The application to *v*- and *w*-velocity are straight forward.

### *3.1. Approximation of convective term of u in x-direction*

The convective term in x-direction: $\partial[uu]^{yz}_{is,j,k}/\partial x$ can be approximated in several ways such as advective form, convective form or skew-symmetric form. In this work we use a convective form

$$
\frac{\partial[uu]^{yz}_{is,j,k}}{\partial x} = 2[u]^{yz}_{is,j,k}\frac{\partial[u]^{yz}_{is,j,k}}{\partial x} + NC \tag{3}
$$

The nonlinear correction (NC) in the above equation correct the linearization of the first term on the rhs. The exact form of this term is long and will not be included here due to limited space. The first term of the linearized convection $[u]^{yz}_{is,j,k}$ is the inherent variable and the second term $\partial[u]^{yz}_{is,j,k}/\partial x$ is computed using sixth-order compact scheme from [4].

*3.2. Approximation of convective term of u in y- and z-directions*

Along the edges of the u-momentum, the convection is a result of the line integral fluxes. In y-direction the net convective fluxes is the difference between the convective flux at the top edge and the bottom edge. At the top edge of u-control surface, the convective flux $[vu]^{z}_{is,j+1/2,k}$ need a similar approximation as equation (3). This flux requires a deconvolution of the surface-average *u* into a line-averaged. We use the sixth-order compact scheme from FVM[5]:

$$\alpha_1[u]^{z}_{is,js-1,k} + [u]^{z}_{is,js,k} + \alpha_2[u]^{z}_{is,js+1,k} = \begin{matrix}\beta_1\left([u]^{yz}_{is,j,k} + [u]^{yz}_{is,j+1,k}\right) \\ +\beta_2\left([u]^{yz}_{is,j-1,k} + [u]^{yz}_{is,j+2,k}\right)\end{matrix} \quad (4)$$

The approximation of diffusive term and the pressure term is straight forward, fourth- and sixth-order approximations can be taken directly from [3] when the approximation is direct e.g. finding differentiation of a surface-averaged from the surface-averaged quantity. Otherwise, if the approximation is a deconvolution type e.g. finding a line-averaged differentiation from the surface-averaged data. The method finding sixth-order nonlinear correction (*NC*) is expanded from [2] but it will not be given here due to limited space.

## 4. Advantage of FSM

The projection method is used to decouple the mass conservation equation from the momentum equation and we solve NSE using the 1st and the 2nd step shown in figure 3. The second step here is equivalent to applying the projection operator **P** to the non-divergence-free velocity obtained in the 1st step. The Fourier transform of the projector is shown in step 4 and the Fourier transform of the whole mass-conservation enforcement is displayed in step 5. Effectively, the accuracy of the mass conservation depends on *i.How good did we compute the mass imbalance and ii.How accurate we solve the Poisson equation* (*the 1st equation in the second step*). The two approximation links together as the numerator and denomination shown in step 5. Together, we call them mass conservation factor ($\mathscr{F}$). The numerator is responsible for preserving the solenoidal part of $\boldsymbol{u}^*$ while the denominator conserve its rotational part. Incorrect pressure means the final field lacks part of $\boldsymbol{\nabla} \times \boldsymbol{u}^*$.

1.Integrate the momentum equation

$u^* = u^n + (\mathscr{H}(u^n) + Gp^n)\Delta t$

2. Projection step

$DG\phi = -\frac{\varrho}{\Delta t} Du^*$

$p^{n+1} = p^n + \phi$

3.Integrate the momentum equation

$P = I - G(DG)^{-1}D$

4. Fourier-Transform of Projection operator

$$\hat{\phi}_{kx,ky,kz} = \frac{\widehat{div}_{kx,ky,kz}}{T_L(kx)kx^2 + T_L(ky)ky^2 + T_L(kz)kz^2}$$

5. Fourier-Transform of Projection method

$$\hat{\phi}_{kx,ky,kz} = \frac{\left(T_{Dx}(kx) + T_{Dy}(ky) + T_{Dz}(kz)\right)\widehat{div}_{kx,ky,kz}}{T_L(kx)kx^2 + T_L(ky)ky^2 + T_L(kz)kz^2}$$

**Figure 3.** Equations related to analysis of projection method.

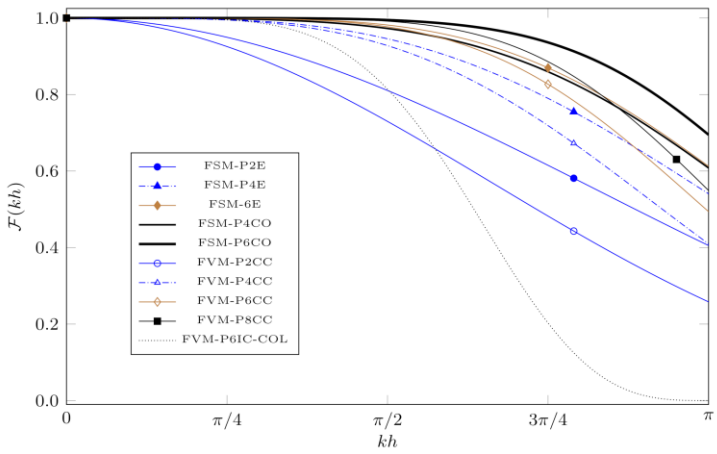


| Method | Mass Conservation Efficiency ($e_m$) | | |
|---|---|---|---|
| | $\epsilon = 0.1$ | $\epsilon = 0.01$ | $\epsilon = 0.001$ |
| FVM-P2CC | 0.291 | 0.090 | 0.028 |
| FSM-P2E | 0.356 | 0.110 | 0.035 |
| FVM-P4CC | 0.548 | 0.296 | 0.165 |
| FSM-P4E | 0.596 | 0.317 | 0.176 |
| FSM-P4CO | 0.688 | 0.391 | 0.222 |
| FVM-P6CC | 0.666 | 0.429 | 0.286 |
| FSM-P6E | 0.706 | 0.446 | 0.296 |
| FSM-L6CO | 0.809 | 0.555 | 0.383 |
| FVM-P8CC | 0.733 | 0.514 | 0.374 |

**Figure 4.** *Left:* Mass conservation factor under projection method; second-order cell-center method (2CC), L4E: explicit fourth-order, L6E:explicit sixth-order, L4C:compact fourth-order, L6C:compact sixth-order, L4CC:fourth-order cell-centered, L6CC:sixth-order cellcentered, L8CC:eight-order cell-centered and L6IC:sixth-order inter-cell. *Right:* Resolving efficiency $e = kh_{max}/\pi$ such that $|1 - \mathscr{F}(kh)| \geq \epsilon$.

Solving NSE on staggered grid usually more accurate than solving them on collocated grid because of the cell-center approximations which have the half-a-cell advantage. This allows a $2\pi$ Nyquist limit (the original data still limited at $\pi$). The collocated grid, on the other hand, must use inter-cell approximations whose resolution is also limited to $\pi$. Under FSM, the approximation of divergence is exact and FSM only need to approximate the Poisson equation. Therefore FSM possess an extraordinary mass-conservation property. In figure 4 we display the mass-conservation factors of the FSM in comparison with other cell-center and inter-cell approximations. We can see in the figure that the factor of the fourth-order inter-cell (IC) approximations flats out at $\pi$ while those of the cell-center (CC) cross the right frame. At the same method and the same order of the truncation error, FSM is much better than FVM on staggered grid which uses cell-center approximations. At low *kh* an *n*-th order FSM and FVM-CC are comparable, but the mass conservation factor of FVM-CC soon falls down while that of the FSM is hanging around the (*n+2*)-th order of FVM-CC. This feature suggests that, when high-wave content of the flow is dominant, the mass conservation of FSM should behave like that of the FVM-CC with two order higher. In order to quantify it, we define the resolving efficiency and tabulated them on the right. The number indicates that, for a given error threshold ($\epsilon$), how much fraction of the wave space the method can capture. Large error threshold, represents the error in high-wave components while small $\epsilon$ represents that in the low-wave components. At the lowest $\epsilon$, the FSM-P4E is roughly 10% less accurate than FVM-P6CC. This difference shrinks to 4% at sixth- and eight-order. Interestingly, the *n*-th compact FSM outperforms (*n+2*)-th order FVM at high-wave components. The fourth-order compact FSM (FSM-P4CO) is only 6% less accurate than FVM-P8CC. The differences become 24% and 40% at the two smaller thresholds. Again, when the high-wave contents are significant like in turbulent flow, the errors will be coming from the high frequency part.

## 5. Performance of the Finite Surface Method

### *5.1 Laminar flow test case*

The first test case consider here is the instability of plane channel flow. The initial parabolic laminar profile is superposed with the eigenmode obtained from Orr-Sommerfeld equations (see figure 5a). Figure 5a shows the evolution of the disturbance's energy. The slope of the curve represents the growth

rate whose analytical value is $G_d = 4.46996E-03$. Under uniform grid, FSM only needs 128 grid in the wall-normal directions to achieve 1E-5 error (0.2% relative error) in the prediction of the growth rate. In comparison, the fourth-order compact FVM[1], would need 173 points. It is found that the sixth-order FSM is 25% faster than the fourth-order compact FVM during the momentum integration. This is because, FSM do not need to interpolate the convective velocity like FVM and thus some computations were saved. Combining the faster speed and the reduction in grid requirement, the sixth-order FSM is faster than the fourth-order FVM by a factor of four, at the same accuracy.

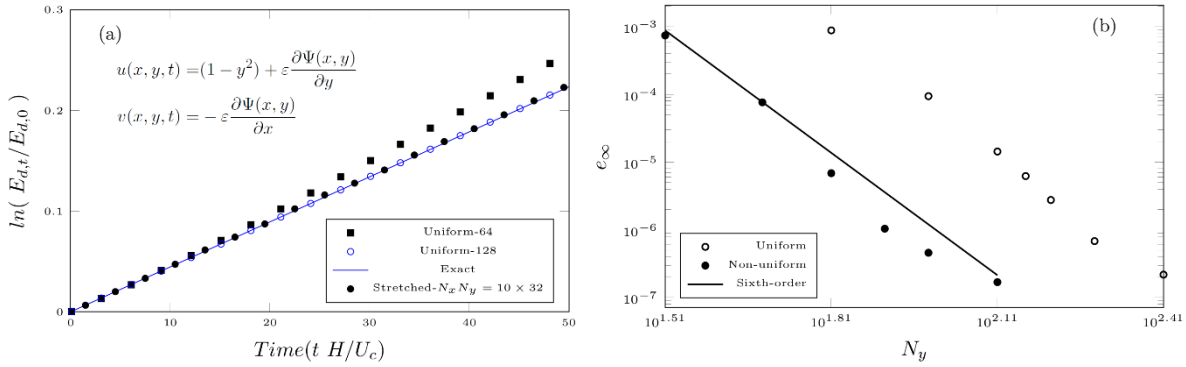


**Figure 5.** Evolution of the perturbations (a) and the error of the perturbations' growth rate from the analytical value.

*5.2 turbulent flow test case*

In the last test case we use direct numerical simulation of a turbulent channel flow with friction Reynolds number= 590 ( bulk flow Reynolds number = 22,000) . The computation domain is $[L_x, L_z, L_y] = [2\pi H, \pi H, 2H]$ in which x, y and z are the streamwise-, spanwise- and wall-normal directions and H is the channel's half-width. The mean streamwise velocity is plotted in figure 6. In our simulation, we fix the pressure gradient which drives the flow. The turbulent interactions generated by the direct numerical simulations will be responsible for producing shear stress. If the turbulence interactions in the numerical simulation are fewer than the reality, the flow rate will be over predicted and if they are becoming too few, the flow could continue accelerating and blow up the simulation. At the lowest resolution $L_x L_z L_y = 32 \times 32 \times 32 = 0.033M$, the numerical scheme cannot capture the shear and the turbulence interactions accurately and result in higher flow rate. Note that the plot is in outer scale. Increasing the resolution by 50% in every direction produce a better result. Surprisingly, the fourth-order FVM[1] need more grid points to match the FSM. Here FVM uses one-third more grid points in every direction, more than the FSM. This number is close to the one predicted in the laminar flow (35%). Still, FVM results is still poorer near the wall despite having more grid. It should be emphasized that the reference solution was simulated with a spectral method on 37.6M grid points which is 340 times more grid points. This does not imply that FSM is more accurate than the spectral method. It just showed that the FSM can capture main features and turbulent interactions sufficiently well, even at this rough resolution. We can predict the necessary resolution that the sixth-order FSM can deliver predictions for the mean and the second-order statistics that are on top of the spectral results. The grid resolution of $[dx, dy, d_{zmin}, d_{zmax}] = [45^+, 15^+, 3^+, 30^+]$ should be sufficient to achieve such predictions.

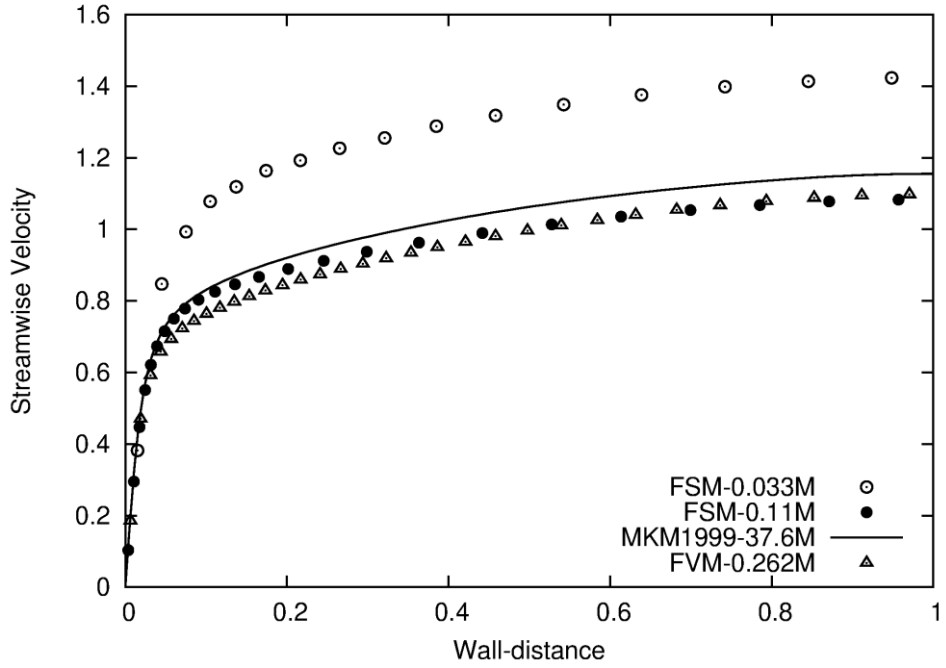


**Figure 6.** Mean streamwise velocity of the turbulent channel flow. The reference solution MKM1999 can be found in [6]

## 6. Conclusion

The finite-surface method is very attractive. This method retains all the good property of staggered grid without the need to create one. The mass-conservation is very good and the Poisson equation created by this method is very compact and can be solved efficiently. It should be noted that the FSM has two finite-volume directions and one finite-difference direction. The finite-difference direction suffers from the usual disadvantages of the FDM. Care must be given to dealiase the error and/or filter out he aliasing error.

## Reference

[1] Hokpunna A and Manhart M. 2010 J. Comput. Phys. p.7545-7570

[2] Knikker R 2009 Int J Numer Methods Fluids. p.1063-1092

[3] Sun Z and Xiao F 2016 *Int. J. Numer. Meth. Fluids*, p.351–375.

[4] Lele S K 1993, J. Comput. Phys. p.16-42.

[5] Kobayashi M H 1999, J. Comput. Phys. p.137-180.

[6] Moser, Kim, Mansour 1999 Phys. of Fluids. p.943.